Variations of the *Mycobacterium abscessus* F-ATP synthase subunit *a-c* interface alter binding and potency of the anti-TB drug bedaquiline

Alexander Krah [a,**], Priya Ragunathan [b], Peter J. Bond [a,c,***], Gerhard Grüber [a,b,*]

[a] *Bioinformatics Institute, Agency for Science, Technology and Research (A*STAR), 30 Biopolis Street, #07-01 Matrix, 138671, Singapore*
[b] *School of Biological Sciences, Nanyang Technological University, 60 Nanyang Drive, 637551, Singapore*
[c] *Department of Biological Sciences, National University of Singapore, 14 Science Drive 4, 117543, Singapore*

ARTICLE INFO

ABSTRACT

The anti-tuberculosis therapeutic bedaquiline (BDQ) is used against *Mycobacterium abscessus*. In *M. abscessus* BDQ is only bacteriostatic and less potent compared to *M. tuberculosis* or *M. smegmatis*. Here we demonstrate its reduced ATP synthesis inhibition against *M. abscessus* inside-out vesicles, including the F_1F_O-ATP synthase. Molecular dynamics simulations and binding free energy calculations highlight the differences in drug-binding of the *M. abscessus* and *M. smegmatis* F_O-domain at the lagging site, where the drug deploys its mechanistic action, inhibiting ATP synthesis. These data pave the way for improved anti-*M. abscessus* BDQ analogs.

1. Introduction

Besides the tuberculosis (TB) causing mycobacteria, *Mycobacterium tuberculosis*, the so-called non-tuberculosis mycobacteria (NTM) have come into focus around the globe as major bacterial pathogens causing respiratory diseases. Among the NTMs the *Mycobacteria abscessus* (*Mab*) complex with its three subclasses called *Mab* subspecies *Mab* subsp. *abscessus*, *Mab* subsp. *massiliense*, and *Mab* subsp. *bolletii*, represents the most frequent rapidly growing NTM related to human respiratory infection [1,2]. The *Mab* complex is difficult to cure with low treatment success rates [1], which in part is due to multi- and extensive drug resistance, in permeability of the cell wall for inhibitors, cleavage and modification of drugs within the pathogen and efficient efflux pumps of the bacterium [3].

As the pathogen is dependent on the oxidative phosphorylation pathway under oxidative and low-oxygen growth conditions, the *Mab* F-ATP synthase has attracted attention as a drug target, reflected by the repurposing of the anti-TB drug Bedaquiline (BDQ) [4]. *Mab*'s F-ATP synthase consists of a F1-sector, composed of the subunits $\alpha_3:\beta_3:\gamma:\epsilon$. The $\alpha_3:\beta_3$-domain includes the catalytic centres, performing ATP synthesis

[5]. This domain is connected via the central stalk subunits γ-ε and a peripheral stalk, composed of subunits $b:b':\delta$, to the proton-translocating F_O-domain subunits *a* and *c* [6,7]. In mycobacteria nine *c* subunits form a ring (*c*-ring), which rotates like a turbine and forms, together with subunit *a*, two half-channels for the translocation of protons from the intermembrane space to the cytoplasm to drive ATP synthesis in the $\alpha_3:\beta_3$-domain [8]. Therefore, blocking the rotation of the turbine prevents transport of protons via the *a-c* half channels. BDQ is composed of four major elements: a quinoline-, a phenyl-, a naphthyl ring and a dimethyl amino (DMA) tether (Fig. 1A). It has been shown to bind to three sites of the F_O-domain of the *Mycobacterium smegmatis* (*Ms*) F_1F_O-ATP synthase, a surrogate of the *M. tuberculosis* enzyme [7]. Five BDQ molecules bind to the *c*-ring while one BDQ molecule binds to the so-called leading- and lagging sites, respectively (Fig. 1B [7]). The leading site is defined as a *c* subunit that has interacted with subunit *a* and received a proton from the periplasm, while the lagging site involves a *c* subunit poised to interact with subunit *a* to deposit a proton into the cytoplasm [7].

Importantly and in contrast to *M. tuberculosis* and *M. smegmatis*, BDQ is not bactericidal and has a 100-times lower growth-inhibitory potency

---

* Corresponding author. Bioinformatics Institute, Agency for Science, Technology and Research (A*STAR), 30 Biopolis Street, #07-01 Matrix, 138671, Singapore.
** Corresponding author.
*** Corresponding author.Bioinformatics Institute, Agency for Science, Technology and Research (A*STAR), 30 Biopolis Street, #07-01 Matrix, 138671, Singapore.
E-mail addresses: kraha@bii.a-star.edu.sg (A. Krah), peterjb@bii.a-star.edu.sg (P.J. Bond), ggrueber@ntu.edu.sg (G. Grüber).
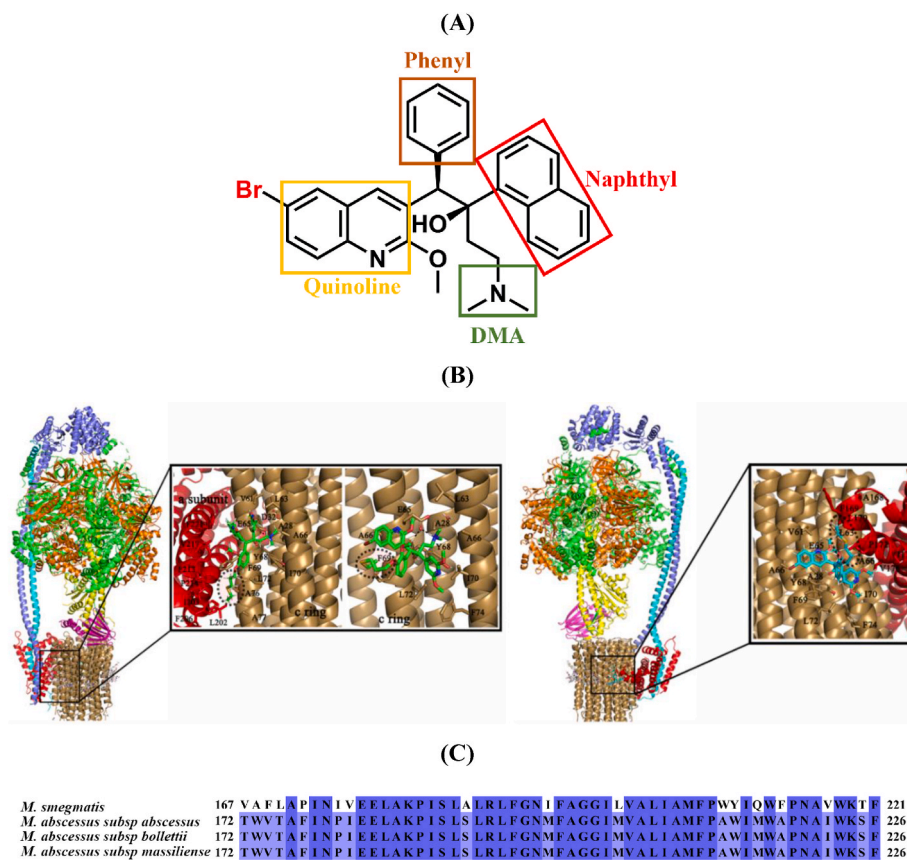
Fig. 1. (*A*) BDQ with its key pharmacophore features (a quinoline-, a phenyl-, a naphthyl ring and a dimethyl amino (DMA) tether). (*B*) The cryo-EM structure of the *M. smegmatis* F_1F_O-ATP synthase shows BDQ's-binding to the so-called leading site and the *c*-ring (*left*) as well as the lagging site (*right*) [7]. The leading site involves a *c* subunit that has just interacted with subunit *a* and picked up a proton from the periplasm, while the lagging site involves a *c* subunit poised to interact with subunit *a* to deposit a proton into the cytoplasm [7]. (*C*) Alignment of the sequence segment of subunit *a* involved in BDQ-binding. The sequences of the three *M. abscessus* subspecies differ from the one from *M. smegmatis*, including the amino acid residues of the leading site.
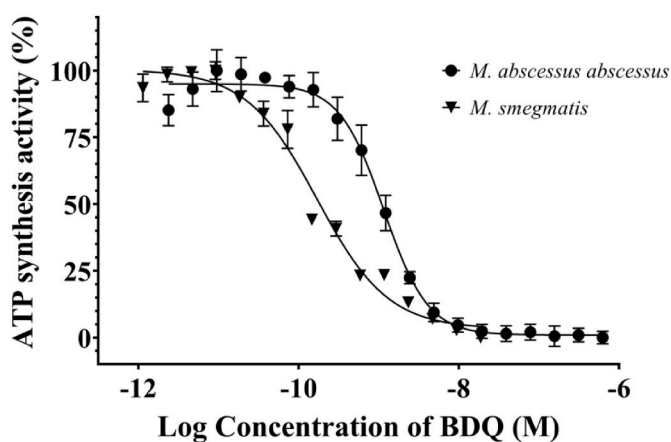

Fig. 2. Inhibition of ATP synthesis by BDQ in *Ms* and *Mab* IMVs using the electron donor NADH. The calculated IC_{50} values of BDQ against *Ms* and *Mab* IMVs are 0.17 ± 0.04 nM and 1.15 ± 0.8 nM, respectively. The ATP synthesis by IMVs was measured as luminescence upon addition of cell titer glo (Promega). The experiments were performed in triplicates. ****: $P < 0.0001$; statistical analysis was carried out for both experiments A-B using one-sample t- and Wilcoxon test.

in *Mab*, which is proposed to be correlated in part with cross resistance in *Mab* efflux pumps [4]. The subunit *a* amino acid sequences of the three *Mab* subspecies *Mab* subsp. *abscessus*, *Mab* subsp. *massiliense*, and *Mab* subsp. *bollettii*, differ from that of *M. smegmatis*, including the

residues at the leading site (Fig. 1C). The pressing questions are whether these changes of the drug against the *Mab* complex are directly correlated with a drop in F-ATP synthase inhibition and whether this may correlate with reduced binding of the drug due to polymorphisms. So far, no studies on *Mab* membranes including the F_1F_O-ATP synthase of the oxidative phosphorylation pathway or structural studies on its F_O-domain are described. In the present study, we demonstrate for the first time BDQ's reduced potency in inhibition of *Mab's* F-ATP synthase using inverted membrane vesicles (IMVs), which correlates with an altered BDQ-binding to the lagging site of the enzyme. We rationalize this via a computational comparison of drug binding in *M. abscessus* and *M. smegmatis*. These data provide insights for structure activity relationship efforts.

2. Materials and methods

2.1. Preparation of inverted membrane vesicles from M. smegmatis and M. abscessus

In order to purify IMVs of *M. smegmatis* mc^2 155 and *M. abscessus subspecies abscessus* for ATP synthesis, cells were cultivated overnight at 37 °C in 7H9 supplemented with 10 % ADC (Albumin - Dextrose – Catalase), 0.5 % glycerol and 0.05 % Tween 80 until it reached OD_{600} 0.6–0.7. The culture was expanded in 200 ml supplemented 7H9 and grown in 1 L shake flasks (180 rpm) until OD_{600} 0.6–0.7. This culture was used to inoculate a 500 ml culture that was grown overnight in 2 L shake flasks (180 rpm) until an OD_{600} of 0.6–0.7. About 5 g (wet weight) of wild-type (WT) *Ms*- and *Mab* cells were resuspended in 20 ml

Table 1
Number of hydrogen bonds and heavy-atom contacts between BDQ and the protein (cut-off 4 Å). Averages and standard deviations for each system were obtained over the whole simulation sampling, in triplicate (300 ns total). Data for *M. smegmatis* were derived from our previous work [11].

a) BDQ positively and E65 negatively charged					
Number of hydrogen bonds			**Number of contacts**		
	M. smegmatis	*M. absecessus*		*M. smegmatis*	*M. absecessus*
Lagging	1.4 ± 0.6	1.3 ± 0.5	**Lagging**	26.3 ± 4.2	27.0 ± 4.1
Leading	1.2 ± 0.5	1.4 ± 0.6	**Leading**	31.4 ± 4.9	27.7 ± 4.9
c-ring	1.2 ± 0.5	1.1 ± 0.4	*c*-ring	22.1 ± 3.5	21.7 ± 3.2
b) BDQ and E65 neutral					
Number of hydrogen bonds			**Number of contacts**		
	M. smegmatis	*M. absecessus*		*M. smegmatis*	*M. absecessus*
Lagging	1.0 ± 0.2	1.0 ± 0.2	**Lagging**	25.0 ± 3.8	24.6 ± 3.7
Leading	0.9 ± 0.3	0.9 ± 0.4	**Leading**	32.1 ± 3.8	29.1 ± 3.8
c-ring	0.8 ± 0.4	0.8 ± 0.4	*c*-ring	19.2 ± 3.4	19.4 ± 3.9

membrane preparation buffer (50 mM MOPS, 2 mM MgCl$_2$, pH 7.5) containing EDTA-free protease inhibitor cocktail (1 tablet in 20 ml buffer, Roche-USA) and 1.2 mg/ml lysozyme. The suspension was stirred at room temperature for 45 min and additionally supplemented with 300 μl 1 M MgCl$_2$ and 50 μl DNaseI (Thermo Fischer, USA), and continued stirring for another 15 min at room temperature. All subsequent steps were performed on ice. Cells were broken by three passages through an ice precooled Model M-110 L Microfluidizer processor (M-110 L) at 18,000 psi. The suspension containing lysed cells was centrifuged at 4200×g at 4 °C for 20 min. The supernatant containing membrane fraction was further subjected to ultracentrifugation 45,000×g at 4 °C for 1 h. The supernatant was discarded, and the precipitated membrane fraction was resuspended in membrane preparation buffer containing 15 % glycerol, aliquoted, snap frozen and stored at −80 °C. The concentrations of the proteins in the vesicles were determined by the BCA method. Inverted membrane vesicles were stored at −80 °C.

2.2. ATP synthesis assay

The reaction mixture for the ATP synthesis assay contained assay buffer (50 mM MOPS [morpholinepropanesulfonic acid]-NaOH, 10 mM MgCl$_2$, pH 7.5), 10 μM ADP, 250 μM P$_i$, and 1 mM NADH. KH$_2$PO$_4$ salt (100 mM) was dissolved in the assay buffer to adjust the concentration of P$_i$; 25 μl of the reaction mixture was added to each well of an opaque, white, 96-well, flat-bottom Nunc plate (Thermo Scientific). BDQ was added to the first well of each row to create 2× the desired highest final concentration. A 16-point 2-fold serial dilution was then carried out starting from the first well. *Ms* and *Mab* inverted membrane vesicles were then added to create a final concentration of 5 μg of protein/ml in 50 μl per well, respectively. Subsequently, the plate was incubated at room temperature for 30 min. At the end of the incubation period, 50 μl of CellTitre-Glo (Promega) was added to each well. The plate was then incubated again for 10 min in the dark at room temperature. Subsequently, luminescence was measured with a Tecan Infinite Pro 200 plate reader (parameters: luminescence, integration time of 500 ms; no attenuation). The level of luminescence correlates with the amount of ATP synthesized by the F-ATP synthase. The graphs of the results were made using GraphPad Prism 8 software.

2.3. Modelling and molecular dynamics simulations (MD) simulations of the F$_O$-domain from M. abscessus bound to BDQ

MODELLER [9] was used to create a homology model of the BDQ bound F$_O$-domain from *M. abscessus* based on the BDQ bound F$_O$-domain from *M. smegmatis* (PDB-ID: 7JGC) [7], constraining the coordinates of common residues and modelling new side chain conformations in areas with residue changes. We simulated three different systems with: 1) BDQ and key-glutamate (E62) both charged (*Mab*); 2) BDQ and E62 both neutral (*Mab*); and 3) the *Ms* F$_O$-domain with no drug present and

key-glutamates (E65) at leading and lagging site deprotonated. Note that the key-glutamate interacting with the essential arginine in subunit *a* was set as charged in all simulation setups. The first simulation setup reflects evidence of the fully charged state in a previous experimental study [10], whereas the second was required for free-energy calculations due to technical issues (see description of free energy methodology below and [11]). The third served as a control simulation to study the solvation of the key-glutamates when there is a full charge present in the membrane phase, as previously reported for the isolated *c*-ring [12,13]; for these control simulations we used the F$_O$ domain from *Ms* for which structural data is available [7]. We used the CHARMM-GUI [14] membrane builder module [15] to insert the protein or protein-drug complex into a 1-palmitoyl-2-oleoyl-sn-glycero-3-phosphocholine (POPC) membrane bilayer. A lipid plug, which has been observed via structural analysis in the cavity of the *c*-ring [16], was modelled as described previously [17]. The system was then solvated and a physiological NaCl concentration was added whilst neutralizing the overall charge of the system. Temperature and pressure were kept constant at 300 K and 1 bar, using the velocity-rescale thermostat [18] and the Parrinello Rahman barostat [19], respectively. We used the CHARMM36m force field for proteins [20], the CHARMM36 force field for lipids [21], the TIP3P water model [22], and CGenFF to generate parameters [23] for BDQ. Simulations were carried out with the GROMACS (v2018 and v2022) simulation suite [24].

An integration time step of 2 fs was used for all simulations. Electrostatic interactions were calculated using the Particle Mesh Ewald method with a 12 Å real space cut-off. Van der Waals interactions were switched after 8 Å and a cut-off of 12 Å was applied. The LINCS [25] algorithm was used to restrain all bonds involving hydrogen atoms. Conventional MD simulations were equilibrated for 20 ns whilst applying position restraints to all protein backbone atoms. Unrestrained production runs were carried out for 100 ns. All conventional MD simulations were carried out in triplicate.

Binding free energy calculations of BDQ bound to the *M. abscessus* and *M. smegmatis* lagging site, where the drug's mode of action occurs, were carried out in the neutral state (drug and key-glutamate). Although the drug and key-glutamate may be charged in a physiological setting [10], this approach was chosen because the charged state of the key-glutamate likely causes artefacts due to potential artefactual solvation of the hydrophobic membrane core in the presence of full charges [12,13] and energetic penalties of the charged carboxylate facing the hydrophobic acyl membrane tails [26]. As a negative control, we also calculated the free energy at the lagging site, when drug and E65 (*Ms*) were set to being charged. The coupling parameter λ was changed from 0 (BDQ fully present) to 1 (BDQ fully annihilated) using 34 windows for the neutral systems and 35 windows for the charged drug/key-glutamate systems. A Beutler soft-core potential [27] was used. Restraints were applied to maintain the drug in the protein-bound state. We simulated each window for 1 ns, discarding the first 100 psas
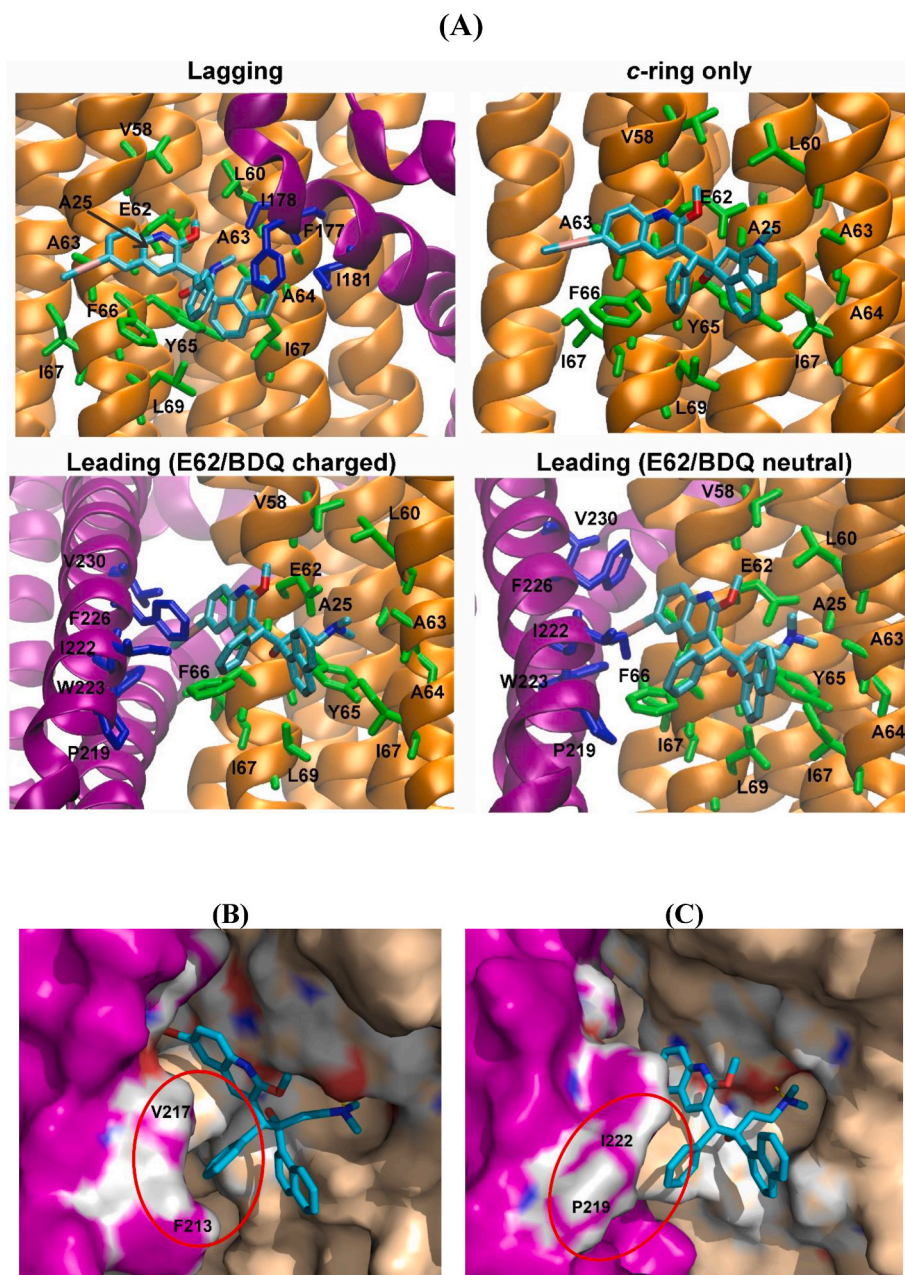
(A)

(B)   **(C)**

Fig. 3. Predicted binding sites for BDQ bound to the *Mab* F$_O$-domain. (*A*) The *c*-ring only, lagging and two possibilities for the leading site of *Mab*, dependent upon the protonation state of E62 and BDQ, are shown. The figure was produced using VMD [31]. (*B*) In the *Ms* leading site residues *a*V217 and *a*F213 form a cavity into which the phenyl ring of BDQ binds favorably. (*C*) Since the *Ms* residues *a*F213 and *a*V217 are substituted by *a*A218 and *a*I222 in the *Mab* subunit *a*, no cavity is formed, leading to a shallow binding area.

equilibration. The Bennet Acceptance Ratio approach [28] was subsequently used to analyse the free energies. We carried out six replicates of the free energy calculations in the neutral state, and three replicas in the charged state; an averaged structure of the three conventional MD simulation replicas was used as input for the free energy calculations.

3. Results and discussion

3.1. BDQ displays lower inhibition of Mab's F$_1$F$_O$-ATP synthase

Firstly, we tested whether the reduced growth inhibition is correlated with a drop in ATP synthesis inhibition of *Mab's* F$_1$F$_O$-ATP synthase by measuring ATP formation of inverted membrane vesicles of *Ms* and *Mab*. As displayed in Fig. 2, the determined BDQ half-maximal inhibitory concentration (IC$_{50}$) of ATP synthesis was 10-times higher in *Mab*- (1.15 ± 0.8 nM) compared to *Ms*-IMVs (0.17 ± 0.04 nM), indicating that BDQ's lower potency of *Mab* growth inhibition correlates with a reduced inhibition of *Mab's* F-ATP synthase.

3.2. MD simulations and free energy calculations provide insights into BDQ binding

To understand this difference at the structural and energetic levels, we performed molecular dynamics (MD) simulations and free energy calculations where the key-glutamate of the *c*-ring, interacting with the DMA moiety, was charged or neutral, as rationalized in our previous work [11]. We first analysed the conventional MD simulations of the *Mab* F$_O$-domain and compared these data with prior MD simulations of

Table 2

Minimum distance of *Mab* subunit *a* and *c* residues to BDQ. Distances are shown for BDQ bound to each site (leading, lagging and *c*-ring only) when drug and key-glutamate are charged or protonated. Distances reported are in Å. Averages and standard deviations for each system were obtained over the whole simulation sampling, in triplicate (300 ns total).

	BDQ (deprotonated)			BDQ (protonated)		
	c-ring	Lagging	Leading	*c*-ring	Lagging	Leading
*c*A25	5.6 ± 0.8	5.2 ± 0.7	5.1 ± 0.6	5.7 ± 0.8	5.2 ± 0.6	5.5 ± 0.7
*c*V58	5.1 ± 0.7	5.2 ± 0.7	5.2 ± 0.8	5.2 ± 0.8	5.6 ± 0.5	5.6 ± 0.5
*c*G59	4.4 ± 0.4	4.3 ± 0.4	4.5 ± 0.5	4.4 ± 0.5	4.5 ± 0.3	4.6 ± 0.4
*c*L60	4.1 ± 0.5	4.2 ± 0.4	4.1 ± 0.4	4.2 ± 0.5	4.5 ± 0.5	4.2 ± 0.6
*c*E62	3.6 ± 0.2	3.5 ± 0.2	3.5 ± 0.1	3.6 ± 0.2	3.6 ± 0.2	3.6 ± 0.2
*c*E62:Oϵx -drug:N	3.2 ± 1.1	2.7 ± 0.1	2.8 ± 0.5	3.4 ± 1.2	2.8 ± 0.2	2.7 ± 0.1
*c*A63	3.6 ± 0.2	3.6 ± 0.2	3.6 ± 0.3	3.6 ± 0.2	3.6 ± 0.2	3.6 ± 0.2
*c*A64	4.1 ± 0.8	3.7 ± 0.2	4.1 ± 0.5	4.3 ± 0.9	3.7 ± 0.2	4.1 ± 0.8
*c*Y65	3.8 ± 0.3	3.8 ± 0.2	3.5 ± 0.1	3.8 ± 0.3	3.7 ± 0.2	3.8 ± 0.2
*c*F66	3.6 ± 0.2	3.6 ± 0.2	3.6 ± 0.3	3.5 ± 0.2	3.5 ± 0.2	3.5 ± 0.2
*c*I67	3.7 ± 0.3	3.7 ± 0.2	3.6 ± 0.3	3.7 ± 0.4	3.7 ± 0.2	3.6 ± 0.2
*c*L69	4.6 ± 1.0	3.9 ± 0.3	4.5 ± 0.8	4.6 ± 1.1	3.9 ± 0.3	4.4 ± 0.6
*c*F71	6.9 ± 1.2	6.1 ± 0.8	7.2 ± 0.9	6.8 ± 1.2	5.6 ± 1.0	6.9 ± 0.9
*a*F177	N/A	3.7 ± 0.4	N/A	N/A	3.7 ± 0.3	N/A
*a*I178	N/A	3.7 ± 0.3	N/A	N/A	3.8 ± 0.2	N/A
*a*I181	N/A	3.8 ± 0.3	N/A	N/A	3.8 ± 0.3	N/A
*a*P219	N/A	N/A	7.2 ± 1.3	N/A	N/A	5.6 ± 1.0
*a*I222	N/A	N/A	4.2 ± 0.8	N/A	N/A	4.0 ± 0.8
*a*W223	N/A	N/A	3.7 ± 1.7	N/A	N/A	2.2 ± 0.5
*a*F226	N/A	N/A	3.3 ± 0.4	N/A	N/A	3.1 ± 0.4
*a*V230	N/A	N/A	4.8 ± 1.6	N/A	N/A	6.6 ± 0.6

BDQ's bound domains from *Ms.* We confirmed the stability of the systems for both organisms by calculating the RMSD for the backbone atoms of the full protein, compared to the initial models. The results show that all systems have a comparable structural stability (Fig. S1). We further calculated the intermolecular interactions of the protein with the drug bound to each site (leading, lagging and c-ring only). While the number of hydrogen bonds is similar at all the three BDQ binding-sites for both organism in either protonation states (Table 1; Fig. 3A), the *Mab* leading site shows less atomic contacts (27.7 ± 4.9) compared to the *Ms* one (31.4 ± 4.9). A statistical analysis of binding residues was performed for the protonated and deprotonated states (Table 2), revealing that the DMA group of BDQ within the *Ms* leading site forms a salt bridge with *c*E65 and makes hydrophobic interactions (*c*L63, *c*A28; Fig. 4). The naphthalene ring makes hydrophobic interactions with *c*I70 and *c*L72 and π-π interaction with *c*Y68. The phenyl ring exhibits π-π interactions with *c*F69 and *a*F213 and hydrophobic contacts with *a*P214 and *a*V217. Meanwhile, the quinoline ring forms π-π (*a*F221) and hydrophobic interactions with *a*W218, *c*I70, *c*A66, *c*A67, *c*G62 and *c*V61. Moreover, the residues F213, P214 and V217 of subunit *a* form a cavity in which the phenyl group binds favorably (Fig. 3B). Such a cavity is missing in the *Mab* structure, since *a*F213 and *a*V217 are substituted by

*a*A218 and *a*I222 in the *Mab* sequence, making the phenyl binding area shallow (Fig. 3C). Interestingly, a lower number of hydrophobic interactions of the naphthalene ring and the DMA moiety can be observed in the *Mab* leading site. In addition, the phenyl ring has π-π interactions with *c*F66 and the quinoline ring makes hydrophobic contacts with *c*I67, *c*A64, *c*L60 and *c*V58. Nevertheless, it should be noted that the ATP hydrolysis activity is latent and barely measurable in mycobacterial species [5]. Thus, the leading site likely does not have any mechanistic relevance to drug action.

The proposed BDQ binding mode to the *Ms* lagging site, where the drug inhibits ATP synthesis, shows that the DAM group is coordinated by a salt bridge with *c*E65 and makes hydrophobic contacts with *c*L63 and *c*A28 (Fig. 4). The naphthalene ring makes π-π (*c*Y68) and hydrophobic interactions (*c*I70 and *c*L72 and *a*V176, *a*I173 and *a*P172). The phenyl ring involves π-π contacts with *c*F69, while the quinoline ring interacts with *c*I70, *c*A66, *c*A67, *c*L63, *c*G62 and *c*V61. The methoxy group of the quinoline ring exhibits a C-H … π interaction with *a*F169. Unlike the *Ms* lagging site, BDQ exhibits a shallow binding with no strong interactions with subunit *a* in the *Mab* lagging site. The DAM group interacts with *c*E62 via a salt bridge and hydrophobic interaction (*c*L60; Fig. 4). The naphthalene ring has hydrophobic (*a*I181, *a*F177, *a*I178, *c*I67 and *c*L69) as well as π-π interactions (*c*Y65). The phenyl ring makes π-π interactions with *c*F66, while the quinoline ring has less hydrophobic contacts compared to its counterpart in the *Ms* lagging-site. Considering the experimental results for the lagging sites (suppression of ATP synthesis), BDQ's slightly different interaction network with subunit *a* in *Mab's* predicted lagging site may be the cause the lower binding affinity to *Mab's* F$_O$-domain (Fig. 1).

To validate our binding site predictions, we aimed to reproduce the experimental binding free energy differences (lagging site inhibition of *Ms*: 0.17 nM (−13.3 kcal/mol) [29] and *Mab*: 1.15 nM (−12.1 kcal/mol) (Fig. 2); ΔΔG$_{bind}$ (*Mab* - *Ms*) = 1.2 kcal/mol). We calculated the binding free energy of the drug bound to the mechanistically relevant *Mab* and *Ms* lagging site. The calculated free energy difference derived from these simulations was 1.3 ± 1.3 kcal/mol and was comparable to the experimental data (1.2 kcal/mol). In these systems, BDQ and E62 were set to be neutral, and we reasoned that any errors arising from the given protonation state should cancel when comparing ΔΔG$_{bind}$ across different organisms. Nevertheless, the charged state may be more relevant to a physiological setting, as indicated in a prior experimental study [10], and we therefore performed control simulations of the drug-free system in which the key-glutamates of the leading and lagging sites of the F$_O$ domain from *Ms* were set to be charged. In this state, spontaneous artefactual solvation of the hydrophobic acyl tail region of the membrane was observed due to the high desolvation energy of the key-glutamate in its charged form [26] in the drug free state, at both the lagging and leading sites (Fig. S2). This phenomenon has also been observed previously in the absence of subunit *a* [12,13]. To further evaluate the influence of the charged key-glutamate upon the results of the free energy calculations, we calculated the binding free energy for BDQ and E65 in their charged states bound to the lagging site of the F$_O$ domain of *Ms*. Our results show a binding free energy of −46.1 ± 2.1 kcal/mol, thus confirming that this approach is not feasible for accurately reproducing the experimental results (−13.3 kcal/mol; Fig. 2). It should be noted that in our previous study [11], the modelled binding modes of TBAJ-876 were found to be in good agreement with a recently released cryo-EM structure [30], thus suggesting that this approach can correctly predict subtle changes in drug binding modes.

These data show that the predicted *c*-ring only site, which is not relevant for the drug-inhibition mechanism, is similar in both species (Fig. 3). In addition, they show the differences of BDQ binding within the *Mab* and *Ms* leading sites, which is likely also not important for the drug's mode of action. Most importantly, the simulations highlight the differences of BDQ's four chemical moieties within the lagging site, where BDQ binding induces ATP synthesis inhibition [7], and thus shed light on the observed difference in drug inhibition in IMVs for both
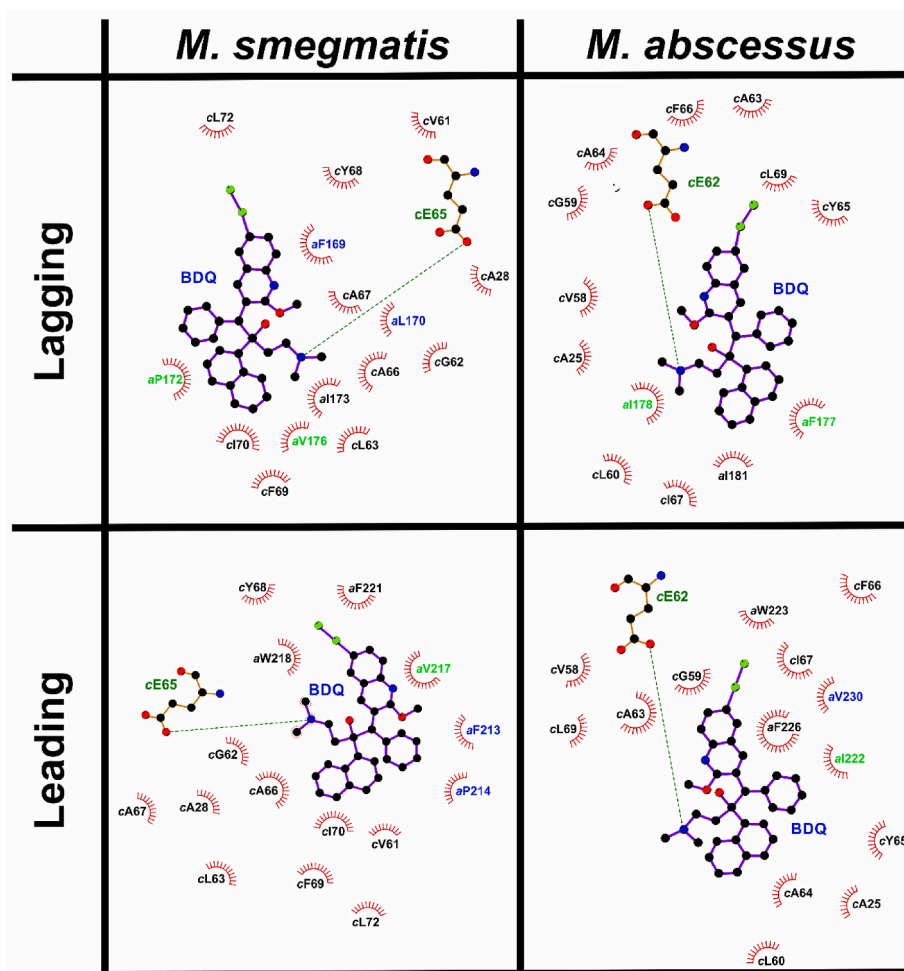
Fig. 4. **Leading and lagging binding sites of BDQ in the F_O domain from *M. smegmatis* and *M. abscessus*.** Ligplot+ [32] representations are shown for BDQ bound to each organism at both inhibition sites. Differences in the binding sites are highlighted in *light green* (substitution in binding residue) or *blue* (altered presence of binding residue). The *c*-ring only site is not shown, as the sites are predicted to be identical. (For interpretation of the references to colour in this figure legend, the reader is referred to the Web version of this article.)

pathogens. Furthermore, while the data do not exclude the possibilities of differences in efflux pump efficiency and selectivity [4] as well as cell permeability between *Mab* and *Ms*, respectively [2], they open the door for new BDQ analogue development with improved potency and bactericidal activity targeting *Mab's* F-ATP synthase.

CRediT authorship contribution statement

Alexander Krah: Conceptualization, Funding acquisition, Investigation, Writing – original draft. **Priya Ragunathan:** Investigation, Writing – review & editing. **Peter J. Bond:** Funding acquisition, Writing – review & editing. **Gerhard Grüber:** Conceptualization, Funding acquisition, Writing – original draft, Writing – review & editing.

Declaration of competing interest

The authors declare that they have no known competing financial interests or personal relationships that could have appeared to influence the work reported in this paper.

Acknowledgements

Appendix A. Supplementary data

Supplementary data to this article can be found online at https://doi.org/10.1016/j.bbrc.2023.149249.

References

[1] S.E. Strollo, J. Adjemian, M.K. Adjemian, D.R. Prevots, The burden of pulmonary nontuberculous mycobacterial disease in the United States, Ann Am Thorac Soc 12 (2015) 1458–1464, https://doi.org/10.1513/ANNALSATS.201503-173OC/SUPPL_FILE/DISCLOSURES.PDF.

[2] M.L. Wu, D.B. Aziz, V. Dartois, T. Dick, NTM drug discovery: status, gaps and the way forward, Drug Discov. Today 23 (2018) 1502–1519, https://doi.org/10.1016/J.DRUDIS.2018.04.001.

[3] N. Wassilew, H. Hoffmann, C. Andrejak, C. Lange, Pulmonary disease caused by non-tuberculous mycobacteria, Respiration 91 (2016) 386–402, https://doi.org/10.1159/000445906.

[4] C. Dupont, A. Viljoen, S. Thomas, F. Roquet-Banères, J.-L. Herrmann, K. Pethe, L. Kremer, Bedaquiline inhibits the ATP synthase in Mycobacterium abscessus and is effective in infected zebrafish, Antimicrob. Agents Chemother. 61 (2017), e01225-17, https://doi.org/10.1128/AAC.01225-17.

[5] C.-F. Wong, C.-Y. Leow, G. Grüber, Cryo-EM structure of the Mycobacterium abscessus F1-ATPase, Biochem. Biophys. Res. Commun. 671 (2023) 140–145, https://doi.org/10.1016/j.bbrc.2023.05.095.

[6] C.F. Wong, W.G. Saw, S. Basak, M. Sano, H. Ueno, H.W. Kerk, D. Litty, P. Ragunathan, T. Dick, V. Müller, H. Noji, G. Grüber, Structural elements involved in ATP hydrolysis inhibition and ATP synthesis of tuberculosis and nontuberculous mycobacterial F-ATP synthase decipher new targets for inhibitors, Antimicrob. Agents Chemother. 66 (2022), e01056-22, https://doi.org/10.1128/aac.01056-22.

[7] H. Guo, G.M. Courbon, S.A. Bueler, J. Mai, J. Liu, J.L. Rubinstein, Structure of mycobacterial ATP synthase bound to the tuberculosis drug bedaquiline, Nature 589 (2021) 143–147, https://doi.org/10.1038/s41586-020-3004-3.

[8] M.G. Montgomery, J. Petri, T.E. Spikes, J.E. Walker, Structure of the ATP synthase from Mycobacterium smegmatis provides targets for treating tuberculosis, Proc. Natl. Acad. Sci. USA 118 (2021), e2111899118, https://doi.org/10.1073/pnas.2111899118.

[9] A. Šali, T.L. Blundell, Comparative protein modelling by satisfaction of spatial restraints, J. Mol. Biol. 234 (1993) 779–815, https://doi.org/10.1006/JMBI.1993.1626.

[10] A.C. Haagsma, I. Podasca, A. Koul, K. Andries, J. Guillemont, H. Lill, D. Bald, Probing the interaction of the diarylquinoline TMC207 with its target mycobacterial ATP synthase, PLoS One 6 (2011), e23575, https://doi.org/10.1371/JOURNAL.PONE.0023575.

[11] A. Krah, G. Grüber, P.J. Bond, Binding properties of the anti-TB drugs bedaquiline and TBAJ-876 to a mycobacterial F-ATP synthase, Curr Res Struct Biol 4 (2022) 278–284, https://doi.org/10.1016/J.CRSTBI.2022.09.001.

[12] H. Gohlke, D. Schlieper, G. Groth, Resolving the negative potential side (n-side) water-accessible proton pathway of F-type ATP synthase by molecular dynamics simulations, J. Biol. Chem. 287 (2012) 36536–36543, https://doi.org/10.1074/jbc.M112.398396.

[13] A. Krah, D. Pogoryelov, T. Meier, J.D. Faraldo-Gomez, On the structure of the proton-binding site in the fo rotor of chloroplast ATP synthases, J. Mol. Biol. 395 (2010) 20–27, https://doi.org/10.1016/j.jmb.2009.10.059.

[14] S. Jo, T. Kim, V.G. Iyer, W. Im, CHARMM-GUI: a web-based graphical user interface for CHARMM, J. Comput. Chem. 29 (2008) 1859–1865, https://doi.org/10.1002/jcc.20945.

[15] E.L. Wu, X. Cheng, S. Jo, H. Rui, K.C. Song, E.M. Dávila-Contreras, Y. Qi, J. Lee, V. Monje-Galvan, R.M. Venable, J.B. Klauda, W. Im, CHARMM-GUI *Membrane Builder* toward realistic biological membrane simulations, J. Comput. Chem. 35 (2014) 1997–2004, https://doi.org/10.1002/jcc.23702.

[16] T. Meier, U. Matthey, F. Henzen, P. Dimroth, D.J. Müller, The central plug in the reconstituted undecameric c cylinder of a bacterial ATP synthase consists of phospholipids, FEBS Lett. 505 (2001) 353–356, https://doi.org/10.1016/S0014-5793(01)02837-X.

[17] A. Krah, J.K. Marzinek, P.J. Bond, Characterizing the hydration properties of proton binding sites in the ATP synthase c-rings of Bacillus species, J. Phys. Chem. B 124 (2020) 7176–7183, https://doi.org/10.1021/acs.jpcb.0c03896.

[18] G. Bussi, D. Donadio, M. Parrinello, Canonical sampling through velocity rescaling, J. Chem. Phys. 126 (2007), 014101, https://doi.org/10.1063/1.2408420.

[19] M. Parrinello, A. Rahman, Polymorphic transitions in single crystals: a new molecular dynamics method, J. Appl. Phys. 52 (1981) 7182–7190, https://doi.org/10.1063/1.328693.

[20] J. Huang, S. Rauscher, G. Nawrocki, T. Ran, M. Feig, B.L. De Groot, H. Grubmüller, A.D. MacKerell, CHARMM36m: an improved force field for folded and intrinsically disordered proteins, Nat. Methods 14 (2016) 71–73, https://doi.org/10.1038/nmeth.4067.

[21] J.B. Klauda, R.M. Venable, J.A. Freites, J.W. O'Connor, D.J. Tobias, C. Mondragon-Ramirez, I. Vorobyov, A.D. MacKerell, R.W. Pastor, Update of the CHARMM all-atom additive force field for lipids: validation on six lipid types, J. Phys. Chem. B 114 (2010) 7830–7843, https://doi.org/10.1021/jp101759q.

[22] W.L. Jorgensen, J. Chandrasekhar, J.D. Madura, R.W. Impey, M.L. Klein, Comparison of simple potential functions for simulating liquid water, J. Chem. Phys. 79 (1983) 926–935, https://doi.org/10.1063/1.445869.

[23] K. Vanommeslaeghe, E. Hatcher, C. Acharya, S. Kundu, S. Zhong, J. Shim, E. Darian, O. Guvench, P. Lopes, I. Vorobyov, A.D. Mackerell, CHARMM general force field: a force field for drug-like molecules compatible with the CHARMM all-atom additive biological force fields, J. Comput. Chem. 31 (2010) 671–690, https://doi.org/10.1002/jcc.21367.

[24] M.J. Abraham, T. Murtola, R. Schulz, S. Páll, J.C. Smith, B. Hess, E. Lindahl, GROMACS: high performance molecular simulations through multi-level parallelism from laptops to supercomputers, SoftwareX 1–2 (2015) 19–25, https://doi.org/10.1016/J.SOFTX.2015.06.001.

[25] B. Hess, H. Bekker, H.J.C. Berendsen, J.G.E.M. Fraaije, LINCS: a linear constraint solver for molecular simulations, J. Comput. Chem. 18 (1997) 1463–1472, https://doi.org/10.1002/(SICI)1096-987X(199709)18:12<1463::AID-JCC4>3.0.CO;2-H.

[26] D. Pogoryelov, A. Krah, J.D. Langer, Ö. Yildiz, J.D. Faraldo-Gómez, T. Meier, Microscopic rotary mechanism of ion translocation in the Fo complex of ATP synthases, Nat. Chem. Biol. 6 (2010) 891–899, https://doi.org/10.1038/nchembio.457.

[27] T.C. Beutler, A.E. Mark, R.C. van Schaik, P.R. Gerber, W.F. van Gunsteren, Avoiding singularities and numerical instabilities in free energy calculations based on molecular simulations, Chem. Phys. Lett. 222 (1994) 529–539, https://doi.org/10.1016/0009-2614(94)00397-1.

[28] C.H. Bennett, Efficient estimation of free energy differences from Monte Carlo data, J. Comput. Phys. 22 (1976) 245–268, https://doi.org/10.1016/0021-9991(76)90078-4.

[29] J.P. Sarathy, P. Ragunathan, J. Shin, C.B. Cooper, A.M. Upton, G. Grüber, T. Dick, TBAJ-876 retains Bedaquiline's activity against subunits c and ε of Mycobacterium tuberculosis F-ATP synthase, Antimicrob. Agents Chemother. 63 (2019), e01191-19, https://doi.org/10.1128/AAC.01191-19.

[30] G.M. Courbon, P.R. Palme, L. Mann, A. Richter, P. Imming, J.L. Rubinstein, Mechanism of mycobacterial ATP synthase inhibition by squaramides and second generation diarylquinolines, EMBO J. 42 (2023), e113687, https://doi.org/10.15252/EMBJ.2023113687.

[31] W. Humphrey, A. Dalke, K. Schulten, VMD: visual molecular dynamics, J. Mol. Graph. 14 (1996) 33–38. http://www.ncbi.nlm.nih.gov/pubmed/8744570.

[32] R.A. Laskowski, M.B. Swindells, LigPlot+: multiple ligand–protein interaction diagrams for drug discovery, J. Chem. Inf. Model. 51 (2011) 2778–2786, https://doi.org/10.1021/ci200227u.